$M_{0.5}Zn_{0.5}Fe_2O_4$ (M = Cu, Co, Mn, Ni) ferrites supported on activated carbon as catalysts for methanol decomposition

R. Ivanova[1]*, B. Tsyntsarski[1], G. Issa[1], I. Spassova[2], D. Kovacheva[2], N. Velinov[3], T. Tsoncheva[1]

[1] *Institute of Organic Chemistry with Centre of Phytochemistry, Bulgarian Academy of Sciences, Acad. G. Bonchev Str. Bl. 9, 1113 Sofia, Bulgaria*
[2] *Institute of General and Inorganic Chemistry, Bulgarian Academy of Sciences, Acad. G. Bonchev Str. Bl. 11, 1113 Sofia, Bulgaria*
[3] *Institute of Catalysis, Bulgarian Academy of Sciences, Acad. G. Bonchev Str. Bl. 11, 1113 Sofia, Bulgaria*

Activated carbon was prepared from cherry stones residues and used as a host matrix of nanosized $M_{0.5}Zn_{0.5}Fe_2O_4$ (M = Cu, Co, Mn, Ni) ferrites. The obtained composites were characterized by Low-temperature nitrogen physisorption, powder X-ray diffraction, Mossbauer and Infrared spectroscopies and temperature-programmed reduction with hydrogen. Their catalytic activity in methanol decomposition as a source of hydrogen was studied in details. The textural analysis demonstrated significant stability of the carbon support during the deposition of the ferrite phase. XRD and Mossbauer data revealed that the loaded metal oxide phase represented a complex mixture of finely dispersed ferrite and substituted magnetite particles. The catalysts based on Cu- and Co-containing ferrites demonstrated fast deactivation in methanol decomposition due to the agglomeration of the active particles and significant structural collapse of the activated carbon. The highly exposed to the reactants Mn^{2+}-Fe^{3+} redox pairs in $Mn_{0.5}Zn_{0.5}Fe_2O_4$ ferrite modification promoted the catalytic process at lower temperature. The observed extremely high catalytic activity for the $Ni_{0.5}Zn_{0.5}Fe_2O_4$ modification was related to the synergistic activity of Ni and ZnO nanoparticles, produced under the reaction medium. The obtained results demonstrated the potential of the activated carbon obtained from waste cherry stones for the preparation of cheap and effective catalysts for hydrogen production.

Key words: methanol decomposition; activated carbon; catalysts; zinc ferrites

INTRODUCTION

Recently, hydrogen was considered as the most effective and clean energy carrier. The only emission produced during the hydrogen burning is water vapor, which can significantly reduce the pollutants and the greenhouse gases in the atmosphere. The main drawback in hydrogen application is its safety storage and supply [1]. Methanol can be successfully used as a hydrogen carrier in gas turbines, fuel cells, vehicles, and industry, because it can easily release hydrogen in situ using different technologies, such as decomposition, steam reforming or partial oxidation [2]. However, the wide application of methanol as a hydrogen source, especially for the portable and mobile installations, requires development of cheap and active under the low operation temperature catalysts. Ferrites are important materials for many technological and industrial applications due to their electrical resistivity, high saturation magnetization, high permeability and tunable catalytic activity [3, 4]. The spinel-type ferrites are generally denoted as

MFe_2O_4, where M is divalent metallic cations [5-12]. In Zn-containing ferrites, the Zn^{2+} ions preferentially occupy the tetrahedral sites. The presence of second metal ion in $ZnFe_2O_4$ can significantly affect its properties [13]. Boudjemaa *et al.* [14] reported that the Co substitution dramatically enhances the catalytic activity of $ZnFe_2O_4$ in hydrogen production by water photo-reduction. Murugesan *et al.* [13] demonstrated the superior properties of $Mn_{0.2}Zn_{0.8}Fe_2O_4$ in high-frequency electronic device applications. Velinov *et al.* [15] reported good catalytic activity in methanol decomposition of Ni-Zn ferrites obtained by spark ignition plasma sintering of nickel-zinc-iron hydroxide carbonate precursors. The significant impact of the reaction medium on the phase transformations in the ferrites was widely studied in [15, 16]. Over the past decades, the attention was focused on the synthesis of nanoferrites [17, 18]. The small size of the nanoparticles enhances the surface area per unit mass, which provides a more active area for the catalytic reactions [19]. However, the nanoferrites possess less cyclic stability due to the structural degradation through the redox process [20]. Improved electrochemical performance of the nanoferrites was reported when

they were incorporated within the carbon-based materials like CNT, porous carbon, and graphene [21, 22]. Among the carbon materials, activated carbon (AC) gains considerable attention due to its chemical inertness, high-temperature stability, and tunable texture and surface characteristics. Activated carbon can be synthesized from renewable and low-cost materials, such as agriculture and industrial residues, which makes it attractive both from the economic and environmental viewpoint [2]. Our previous investigation showed that $Ni_xZn_{1-x}Fe_2O_4$ modified activated carbons obtained from peach stones and coal treatment by-products possess a significant potential for sustainable environmental protection as cheap and effective catalysts for hydrogen production [23].

The present investigation is focused on the preparation of nanosized $M_{0.5}Zn_{0.5}Fe_2O_4$ (M = Cu, Co, Mn, Ni) ferrites, hosted in activated carbon obtained from waste biomass (cherry stones). The effect of the carbon support on the formation of the catalytic active phase was discussed in detail using various physicochemical techniques, such as Boehm method, low-temperature nitrogen physisorption, powder X-ray diffraction, Mossbauer spectroscopy, Infrared spectroscopy and temperature-programmed reduction with hydrogen. Their potential application as catalysts for methanol decomposition to hydrogen and carbon monoxide was also investigated.

EXPERIMENTAL

Synthesis of catalysts

Nanoporous carbon from cherry stones was prepared as follows: The precursor (30 g crushed cherry stones, size 1-3 mm) was subjected to carbonization at 973 K and subsequent physical activation with water vapor in a stainless-steel vertical reactor at 1173 K for 1 h. The obtained activated carbon was modified by incipient wetness impregnation with methanol solutions of $Fe(NO_3)_3 \cdot 9H_2O$, $Zn(NO_3)_2 \cdot 6H_2O$ and/or $Ni(NO_3)_2 \cdot 6H_2O$, $Co(NO_3)_2 \cdot 6H_2O$, $Cu(NO_3)_2.3H_2O$, $Mn(NO_3)_2.4H_2O$ in appropriate ratio as described in [23]. After the impregnation step, the samples were dried at room temperature for 24 h and then, treated in vacuum at 323 K for 2 h. The metal precursor was decomposed in nitrogen at 773 K for 2 h. The metal content in the samples was 8 wt.%, the Fe/(Zn+M) molar ratio was 2 and the Zn/ M molar

ratio was 1. The modifications were denoted as $M_{0.5}Zn_{0.5}Fe_2O_4/AC$, where M was Cu, Co, Mn, Ni, and AC is the carbon support.

Methods of investigation

The textural characteristics of the materials were studied by low-temperature nitrogen adsorption in a Quantachrome Instruments NOVA 1200e (USA) apparatus. The specific surface area was determined from Brunauer Emmett Teller (BET) equation, the total pore volume was obtained at a relative pressure of 0.99, the micropores volume was elucidated by the t-plot method. The amount of surface oxygen-containing acidic functional groups was determined following Boehm method and the total number of basic sites was determined by titration with HCl [23]. Powder X-ray diffraction (XRD) study was performed on a Bruker D8 Advance diffractometer (Bruker AXS GmbH, Germany) with Cu Kα radiation and a LynxEye detector with a constant step of 0.02°2θ and counting time of 17.5 s per step. The mean crystallite sizes were determined by the Topas-4.2 software. The Fourier Transform Infrared Spectroscopic (FTIR) study was performed on a Bruker Vector 22 FTIR spectrometer (Bruker Optics, Germany) at a resolution of 1 cm⁻¹ and accumulating scans of 64 using KBr technique in the range of 4000-400 cm⁻¹. The Mössbauer measurements were performed with a Wissel (Wissenschaftliche Elektronik GmbH, Germany) electromechanical spectrometer working in a constant acceleration mode at room temperature (RT). A [57]Co/Rh source (Activity @ 20 mCi) and Fe standard were used. The experimentally obtained spectra were fitted with WinNormos. The parameters of hyperfine interaction such as isomer shift (IS) line, quadruple splitting (QS), hyperfine magnetic field (Heff), width (FWHM), relative weight (G) of the partial components in the spectra were determined. The Temperature Programmed Reduction/Thermo-gravimetric (TPR/TG) study was performed on a Setaram TG 92 apparatus (SETARAM Instrumentation, France) in a mixture of hydrogen and argon (100 cm³min⁻¹, volume ratio $H_2:Ar =1$) and heating rate of 5 Kmin⁻¹.

Catalytic test

Methanol decomposition was carried out in a flow-type microreactor (55 mg of catalyst diluted with crash glass (weight ratio of 1:3) at 1.57 kPa partial pressure of methanol and WHSV of 100 h⁻¹.

Before the catalytic test, the samples were pre-treated in situ for 1 h at 373 K in argon. Methanol dosage was achieved by a saturator kept at 273 K using argon as a carrier gas. The experimental data were collected under a thermo-programmed regime of heating rate of 2 K/min within the temperature range of 423–770 K. On-line gas chromatographic analyses were performed on an HP 5890 apparatus equipped with flame ionization (FID) and thermo-conductivity (TCD) detectors, on a PLOT Q column (J&W HP-PLOT Q GC Column, 30 m, 0.53 mm, 40.00 µm, 7 inch cage). The results were calculated using the method of absolute calibration on the base of carbon material balance. The methanol conversion was calculated as $X = ((C_{ini} - C_{cur})/C_{ini}) \times 100$, where C_{ini} and C_{cur} were the initial and current detected amounts of methanol, respectively. The selectivity to i product from methanol conversion was calculated as $Y_i/X \times 100$, where Y_i was its yield determined from $C_i/C_{ini} \times 100$ (C_i was the amount of i product).

RESULTS AND DISCUSSION

Nitrogen physisorption

Low-temperature nitrogen physisorption analyses of parent activated carbon and all modifications revealed presence of micro-and mesopores (Fig. 1, Table 1). The carbon support possessed relatively high specific surface area and pore volume. After the modification, no significant decrease in the BET surface area and pore volume were observed, which evidences absence pore-blocking due to the deposition of the active phase. No substantial structural changes of the support

during the modification procedure could be assumed. The increase in the V_{mic}/V_{mes} ratio for Mn$_{0.5}$Zn$_{0.5}$Fe$_2$O$_4$/AC as compared to the parent AC evidences predominant location of the metal species into the mesopores. The preservation of V_{mic}/V_{mes} ratio for Cu$_{0.5}$Zn$_{0.5}$Fe$_2$O$_4$/AC and Ni$_{0.5}$Zn$_{0.5}$Fe$_2$O$_4$/AC indicates almost random distribution of the metal species into the micro/mesopores of the carbon support or their deposition on the external surface.
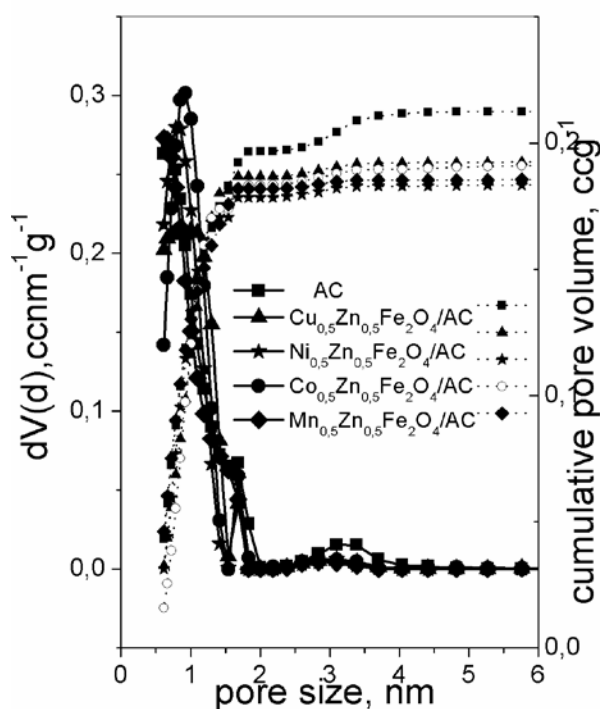

Fig. 1. Pore size distribution of the studied samples.

Table 1. Nitrogen physisorption data.*

Sample	S$_{BET}$, m^{2}g^{-1}	S$_{mic}$, m^{2}g^{-1}	V$_{mic}$, cm^{3}g^{-1}	V$_t$, cm^{3}g^{-1}	V$_{mic}$/V$_{mes}$
AC	488	430	0.18	0.23	3.6
Cu$_{0.5}$Zn$_{0.5}$Fe$_2$O$_4$/AC	465	417	0.17	0.22	3.4
Ni$_{0.5}$Zn$_{0.5}$Fe$_2$O$_4$/AC	454	407	0.16	0.21	3.2
Mn$_{0.5}$Zn$_{0.5}$Fe$_2$O$_4$/AC	453	411	0.17	0.21	4.3
Co$_{0.5}$Zn$_{0.5}$Fe$_2$O$_4$/AC	459	403	0.16	0.23	2.3

* BET surface area (S$_{BET}$), surface area of micropores (S$_{mi}$), micropores pore volume (V$_{mi}$), total pore volume (V$_t$)

Table 2. Phase composition, unit cell parameters and average crystallite size for the modifications.

Sample	Phase composition	Cell parameters, Å	Crystallite size, nm
Cu$_{0.5}$Zn$_{0.5}$Fe$_2$O$_4$/AC	Spinel, Fd-3m (97%)	8.425	21
	Cu$_2$O, Pn-3m (3%)	4.284	16
Ni$_{0.5}$Zn$_{0.5}$Fe$_2$O$_4$/AC	Spinel	8.404	34
Mn$_{0.5}$Zn$_{0.5}$Fe$_2$O$_4$/AC	Spinel	8.465	21
Co$_{0.5}$Zn$_{0.5}$Fe$_2$O$_4$/AC	Spinel	8.420	20
	Traces ZnO (<1%)		

Powder X-ray diffraction (XRD)

The structure and phase composition of the samples was studied by powder X-ray diffraction (XRD) (Fig. 2, Table 2). The main diffraction peaks at 30°, 35°, 43°, 56°, 62° 2Θ were attributed to (220), (311), (222), (400), (422), (511) and (440) planes of a single-phase cubic spinel structure of Fd3m space group (JCPDS card no. 22-1012.). The average size of the spinel crystallites, calculated by Scherrer equation, was in the range of 16-34 nm. The diffraction peaks of the Ni-containing sample were narrower and highly intensive suggesting presence of larger crystallites. This is in accordance with [24] where the facile effect of Ni^{2+} ions on spinel grain growth was reported. The obtained unit cell parameters were lower than the reported in the literature for $ZnFe_2O_4$ [14] (Table 2). This effect could be attributed to the substitution of bigger Zn^{2+} ions by smaller Ni^{2+}, Cu^{2+} Co^{2+} ones in the spinel structure [14]. Boudjemaa *et. al.* [14] reported that the lattice parameter of the spinel was not directly correlated with the ionic radius of the cation in the ternary ferrites since it depends not only on the radius of cation but also vary with the distribution of the cations over the octahedral and tetrahedral sites. Thus, changes in cation distribution could be assumed in the case of manganese modification.
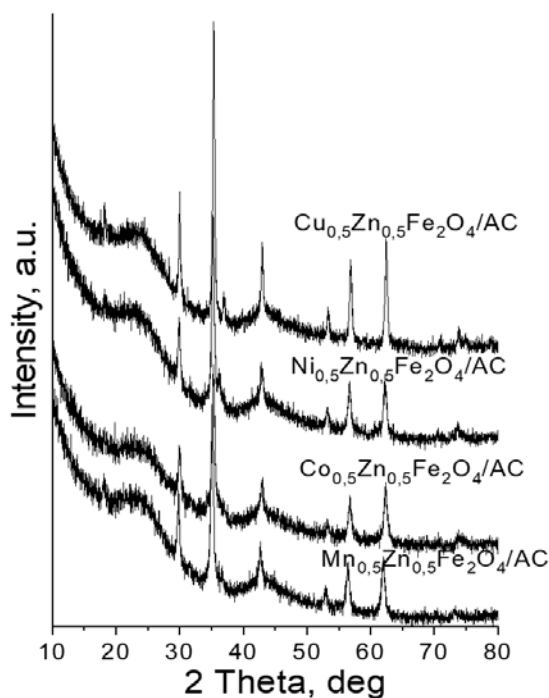

Fig. 2. XRD patterns of the studied samples.

Fourier transform infrared spectroscopy

FTIR analysis (Fig. 3 a, b) was performed to elucidate the chemical structure and functional groups of the materials. The broad band at about 3600-3000 cm^{-1} in the spectra of the carbon support (not shown) was ascribed to residual water or hydrogen-bonded O-H stretching vibrations [25]. The band at 1731 cm^{-1} and the broad absorption band at about 1600 cm^{-1} were assigned to the C=O stretching vibration in carbonyl groups (C=O), and C=C bonds in the aromatic structure, respectively (Fig. 3 a). The bands near 1420 cm^{-1} were due to the CH_2 asymmetric deformation and aromatic C−C stretching vibrations. The bands between 1373 and 1160 cm^{-1} were assigned to phenol O−H bending, C−O stretching in carboxylic acids, alcohols, esters, and phenol groups [25]. Table 3 shows information for the amount of carbon surface functional groups, obtained by Boehm method and by titration with HCl. The carbonyl groups dominate on the surface, which well correlated with the data from the FTIR analysis. FTIR spectra of all ferrite modifications (Fig. 3 b) consisted of two additional peaks at ∼580 cm^{-1} and below 400 cm^{-1} which could be assigned to M-O vibrations of metal ions in tetrahedral and octahedral positions in the ferrites, respectively [26]. The change in the position of the main FTIR bands after the modification of AC evidenced the interaction of metal species with the surface functional groups and carbon basal planes [27].

Moessbauer spectroscopy

The values of the line width (FWHM), isomer shift (IS), quadruple splitting (QS), hyperfine magnetic field (Heff) and relative weight of each component (G) are listed in Table 4. The obtained Mössbauer spectra were fitted by considering two hyperfine magnetic sextets and a paramagnetic doublet. It is well-known fact that the magnetic parameters obtained for sextets and doublets are the characteristics of Fe ions occupying tetrahedral (A) as well as octahedral [B] sites, respectively. Note that, the observed values of quadrupole splitting except for doublet were very small. This could be attributed to the maintained cubic symmetry between Fe^{3+} and surrounding ions [28]. The sextets denoted as Sx1 and Sx2 with IS=0.29 mm/s and IS=0.66 together with QS∼0 mm/s corresponded to Fe^{3+} and $Fe^{2.5+}$ ions in tetrahedral and octahedral positions within the spinel lattice,
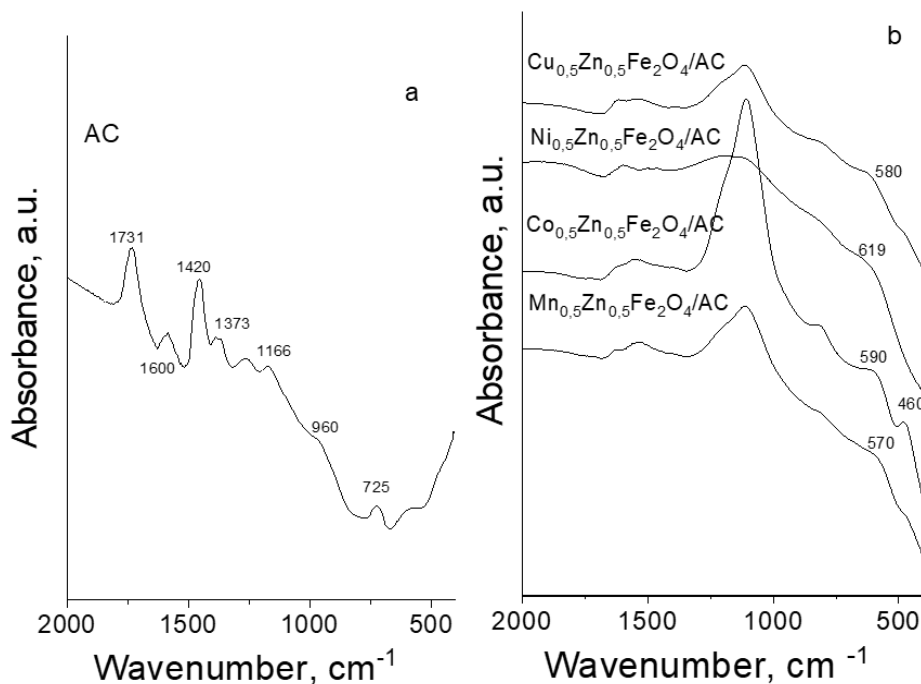
Fig. 3. FTIR spectra of carbon support (a) and all modifications (b).

Table 3. Surface functional groups, determined by the Boehm method.

Sample	Acidic groups (mmol g^{-1})				Total basic groups (mmol g^{-1})
	Carboxylic	Lactone	Phenolic	Carbonyl	
AC	BDL	BDL	0.10	2.5	1.08

Table 4. Moessbauer parameters of all modifications.[a]

Sample	Components	IS, mm/s	QS, mm/s	Heff, T	FWHM, mm/s	G, %
$Cu_{0.5}Zn_{0.5}Fe_2O_4/AC$	Sx1-(Cu,Zn)$_x$Fe$_{3-x}$O$_4$	0.29	0.00	39.5	1.82	39
	Sx2- (Cu,Zn)$_x$Fe$_{3-x}$O$_4$	0.66	0.00	37.9	2.00	38
	Db-Fe^{3+}	0.34	0.50	-	0.54	22
$Ni_{0.5}Zn_{0.5}Fe_2O_4/AC$	Sx1-(Ni,Zn)$_x$Fe$_{3-x}$O$_4$	0.29	0.00	44.5	0.98	35
	Sx2-(Ni,Zn)$_x$Fe$_{3-x}$O$_4$	0.66	0.00	39.8	1.85	48
	Db-Fe^{3+}	0.34	1.23	-	1.03	17
$Mn_{0.5}Zn_{0.5}Fe_2O_4/AC$	Sx1-(Mn,Zn)$_x$Fe$_{3-x}$O$_4$	0.29	0.00	37.3	1.45	36
	Sx2-(Mn,Zn)$_x$Fe$_{3-x}$O$_4$	0.66	0.00	34.2	2.00	53
	Db-Fe^{3+}	0.36	1.14	-	1.03	11
$Co_{0.5}Zn_{0.5}Fe_2O_4/AC$	Sx1-(Co,Zn)$_x$Fe$_{3-x}$O$_4$	0.29	0.00	44.9	1.60	36
	Sx2-(Co,Zn)$_x$Fe$_{3-x}$O$_4$	0.66	0.00	40.9	1.88	43
	Db-Fe^{3+}	0.34	0.89	-	0.71	21
$Cu_{0.5}Zn_{0.5}Fe_2O_4/AC$ *	Sx1- χ-Fe$_5$C$_2$	0.22	0.07	18.7	0.58	58
	Sx2- χ-Fe$_5$C$_2$	0.17	0.07	10.9	0.70	21
	Sx3 - χ-Fe$_5$C$_2$	0.25	0.07	21.8	0.38	21

* after catalytic test; [a] isomer shift (IS) line, quadruple splitting (QS), hyperfine magnetic field (Heff), width (FWHM), relative weight (G).

respectively [23]. These results well correlate with the data obtained by powder X-ray diffraction (Fig. 2, Table 2) for the purity of the spinel phase. The doublets had characteristic parameters for Fe^{3+} in octahedral coordination in paramagnetic or superparamagnetic phases. In the spectra of the studied samples, the doublets had higher values of quadrupole splitting. A possible reason for this

97

could be due to the presence of defects in the ferrite structure, due to the changes in the dispersion of the oxide particles [28].

Temperature programmed reduction-thermogravimetric analyses (TPR-DTG)

In Fig. 4 are shown TPR profiles for various modifications in the 400 - 850 K range. All modifications exhibited weight loss above 550 K and several reduction effects with different shape and position were detected up to 800 K. In accordance with the data from the XRD analyses, the significant differences in the TPR profiles could be assigned to the variations in the dispersion of the active phase (Fig. 2, Table 2). The reduction transformations occurred in the ranges around 650-700 K and 750-800 K and their intensity strongly depended on the type of the second metal component. According to the literature, the high-temperature effect could be related to the reduction of $Fe^{3+} \rightarrow Fe^{2.5+}$ to metallic iron [23]. The lack of well-distinguished reduction effects for $Mn_{0.5}Zn_{0.5}Fe_2O_4/AC$ and $Co_{0.5}Zn_{0.5}Fe_2O_4/AC$ modifications could be due to the presence of manganese and cobalt ions in a lower oxidation state [29, 30]. The reduction profile of $Cu_{0.5}Zn_{0.5}Fe_2O_4/AC$ exhibited two well-distinguished peaks at about 674 K and 776 K indicated co-existence of Cu_2O and partially reduced mixed oxide phase, which formation was favored by the carbon support. For $Ni_{0.5}Zn_{0.5}Fe_2O_4/AC$ sample the reduction transformations were shifted to higher temperature. All these observations confirmed the crucial role of carbon support on the state and dispersion of the loaded ferrite phase [23].

Catalytic study

In Fig. 5 are presented the temperature dependencies of methanol decomposition on various ferrite-supported materials. Most of the samples initiate the catalytic process above 600 K. All materials possessed above 80% selectivity to CO. Methane (up to 15%) and CO_2 (up to 10%) were detected as by-products. Despite the catalytic process started at the lowest temperature for $Mn_{0.5}Zn_{0.5}Fe_2O_4/AC$, its catalytic activity increased extremely slowly with the temperature increase. The shift of the conversion curve of $Ni_{0.5}Zn_{0.5}Fe_2O_4/AC$ to lower temperature demonstrated its higher catalytic activity.
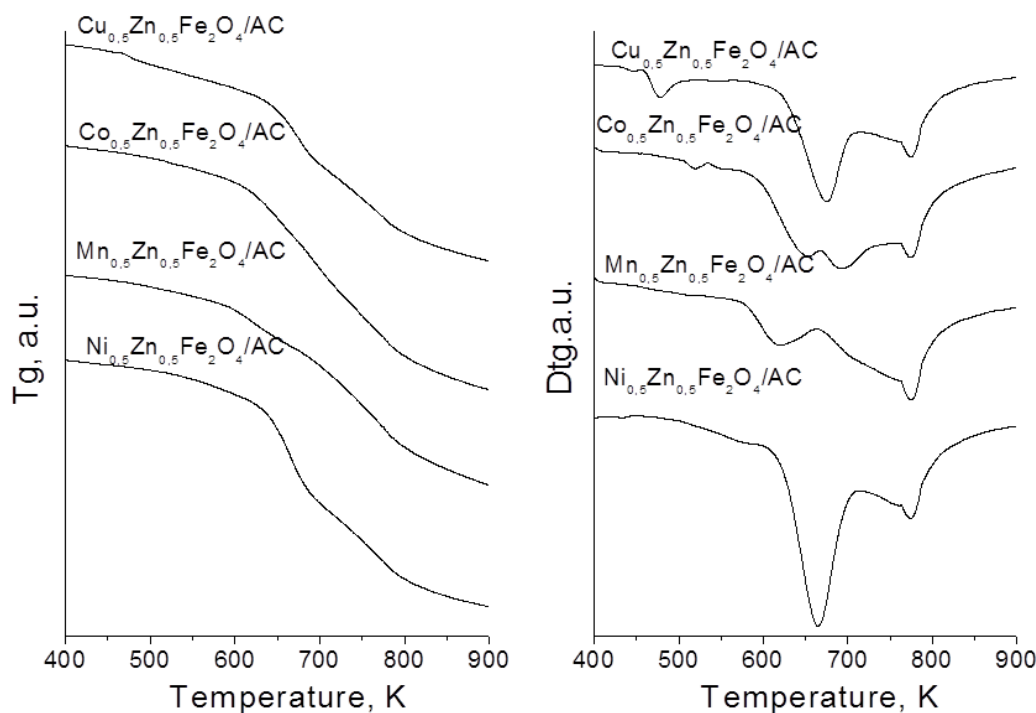
Fig. 4. TPR profiles for all samples.
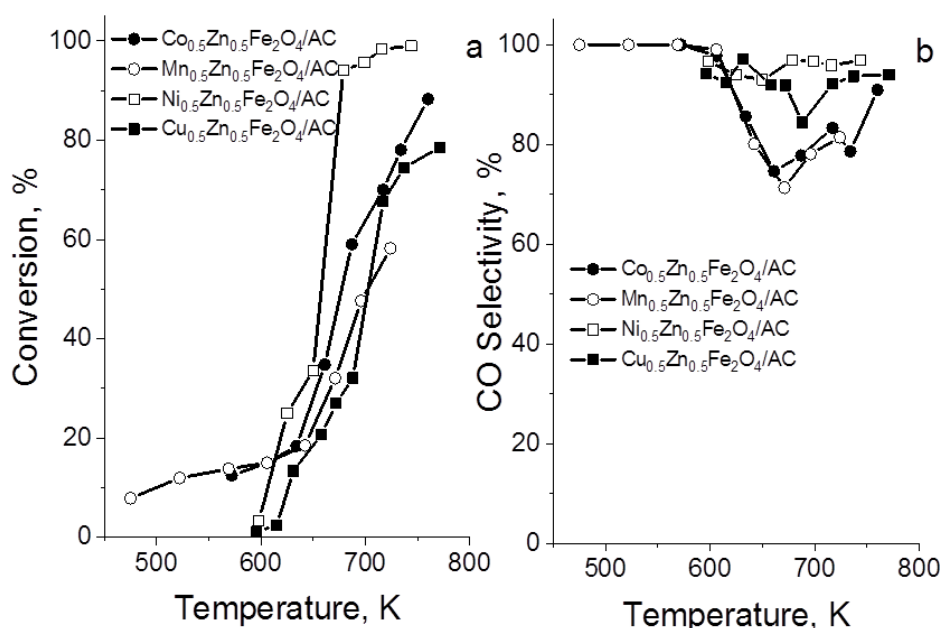
Fig. 5. Temperature dependencies of methanol decomposition (a) and selectivity to CO (b) on various modifications.

The changes in the slope of the conversion curves for the Cu- and Co-based modifications indicated fast deactivation of the catalysts due to irreversible changes with them. The TPR profiles (Fig. 4) and the Moessbauer spectra of the samples after the catalytic test (Table 4) indicated facile reduction decomposition of the loaded ferrite phases, which occurred both by carbon support and reduction reaction medium. These changes occurred not only during the preparation procedure but also during the catalytic test. As a result, a complex mixture of metals, metal oxides, and carbide phases was formed (Table 4). Thus, the catalytic behavior of the samples represented a superposition of the own catalytic activity of different phases. We can propose that the extremely high catalytic activity of $Ni_{0.5}Zn_{0.5}Fe_2O_4/AC$ was due to the synergistic action of metallic Ni and ZnO phases, where ZnO played a role of "reservoir" of the formation of methoxy intermediates and Ni promoted the C-H scission in them with the formation of H_2 and CO [23]. The fast reduction of Cu-based materials even during the preparation procedure rendered difficult the formation of ferrite-like structures and facilitated the formation of Cu_2O phase (Table 2). Further reduction and fast agglomeration of metallic Cu particles was most probably the main reason for its lowest catalytic

activity and well-defined tendency for rapid deactivation. Similar, but less pronounced changes were responsible for the behavior of the $Co_{0.5}Zn_{0.5}Fe_2O_4/AC$ modification. We suggest, that the highly exposed to the reactants Mn^{2+}-Fe^{3+} redox pairs, situated at octahedral position in $Mn_{0.5}Zn_{0.5}Fe_2O_4$ initiated the reaction at significantly lower temperature, but the decomposition of the ferrite to MnO and ZnO phases under the reaction medium resulted in a decrease of the catalytic activity at higher temperatures.

CONCLUSION

Nanosized $M_{0.5}Zn_{0.5}Fe_2O_4$ (M = Cu, Co, Mn, Ni) ferrites supported on activated carbon from waste biomass were successfully prepared by incipient wetness impregnation and tested as catalysts in methanol decomposition. The results of the physicochemical analyzes show that the active phase on the carbon support is a complex mixture of finely dispersed metal oxide phases, which changes significantly by the influence of the reaction medium. The highest catalytic activity for $Ni_{0.5}Zn_{0.5}Fe_2O_4$ modification was related to the synergistic activity of metallic Ni and ZnO particles, which were produced during the reduction transformations of the ferrite phase.

REFERENCES

1. M. Luo, Y. Yi, S. Wang, Z. Wang, M. Du, J. Pan, Q. Wang, *Renew. Sustain. Energy Rev.,* **81**, 3186 (2018).
2. T. S. Tsoncheva, A. B. Mileva, B. G. Tsyntsarski, D. G. Paneva, I. P. Spassova, D. G. Kovacheva, N. I. Velinov, D. B. Karashanova, B. N. Georgieva, N. V. Petrov, *Biomass Bioenergy,* **109**, 135 (2018).
3. N. M. Deraz, M. M. Hessien, *J. Alloy. Compd.*, **475**, 832 (2009).
4. M. Khodaei, S. A. Ebrahimi, Y. J. Park, J. M. Ok, J.S. Kim, J. Son, S. Baik, *J. Magn. Magn. Mater.*, **340,** 16 (2013).
5. A. V. Humbe, J. S. Kounsalye, S. B. Somvanshi, A. Kumar, K. M. Jadhav, *Mater. Adv.*, **1**, 880 (2020).
6. A. S. Albuquerque, M. V. Tolentino, J. D. Ardisson, F. C. Moura, R. de Mendonca, W. A. Macedo, *Ceramic Int*., **38**, 2225 (2012).
7. S. Nair, M. Kurian, *J. Environ. Chem. Eng.*, **5**, 964 (2017).
8. S. A. Jadhav, S. B. Somvanshi, M. V. Khedkar, S. R. Patade, K. Jadhav, *J. Mater. Sci. Mater. Electron.,* **31,** 11352 (2020).
9. R. Sharma, P. Thakur, P. Sharma, V. Sharma, *J. Alloys Compd.*, **704,** 7 (2017).
10. S. Debnath, R. Das, *J. Mol. Struct*., **1199**, 127044 (2020).
11. D. D. Andhare, S. R. Patade, J. S. Kounsalye, K. Jadhav, *Physica B*, **583,** 412051 (2020).
12. C. Murugesan, G. Chandrasekaran, *J. Supercond. Nov. Magnetism*, **29**, 2887 (2016).
13. C. Murugesan, K. Ugendar, L. Okrasa, J. Shen, G. Chandrasekaran, *Ceramic Int*., **47**, 1672 (2021).
14. A. Boudjemaa, I. Popescu, T. Juzsakova, M. Kebir, N. Helaili, K. Bachari, I.-C. Marcu, *Int. J. Hydrog. Energy,* **41,** 11108 (2016).
15. N. I. Velinov, E. D. Manova, T. S. Tsoncheva, C. Estournès, D. G. Paneva, K. K. Tenchev, V. S. Petkova, K. V. Koleva, B. N. Kunev, I. G. Mitov, *Solid State Sci.,* **14**, 1092 (2012).
16. K. V. Koleva, N. I. Velinov, T. S. Tsoncheva, I. G. Mitov, B. N. Kunev, *Bulg. Chem. Commun.*, **45**, 434 (2013).
17. S. B. Somvanshi, S. A. Jadhav, M. V. Khedkar, P. B. Kharat, S. More, K. Jadhav, *Ceram. Int.,* **46,** 8640 (2020).
18. M. Ahmed, N. Okasha, S. El-Dek, *Nanotechnology*, **19**, 065603 (2008).
19. M. R. Chandra, T. S. Rao, H. S. Kim, S. V. Pammi, N. Prabhakarrao, *J. Asian Ceram. Soc.*, **5**, 436 (2017).
20. A. Tabrizi, N. Arsalani, A. Mohammadi, H. Namazi, L. Saleh, *New J. Chem.*, **41,** 4974 (2017).
21. S. Chella, P. Kollu, E. Vara, P. Komarala, S. Doshi, M. Saranya, S. Felix, R. Ramachandran, P. Saravanan, V. L. Koneru, V. Venugopal, S. K. Jeong, A. N. Grace, *Appl. Surf. Sci*., **327**, 27 (2015).
22. G. Wang, L. Zhang, J. Zhang, *Chem. Soc. Rev.*, **41**, 797 (2012).
23. T. S. Tsoncheva, B. G. Tsyntsarski, R. N. Ivanovaa, I. P. Spassova, D. G. Kovacheva, G. S. Issa, D. G. Paneva, D. B. Karashanova, M. D. Dimitrov, B. N. Georgieva, N. V. Petrov, I. G. Mitov, N. V. Petrov, *Micropor. Mesopor. Mater.*, **285**, 96 (2019).
24. A. Manohar, K. Chintagumpala, K. Kim, *Ceram. Int.,* **47**, 7052 (2021).
25. T. S Tsoncheva, A. B. Mileva, S.P. Marinov, D. G. Paneva, N. V. Velinov, I. P. Spassova, A. D. Kosateva, D. G. Kovacheva, N. V. Petrov, *Micropor. Mesopor. Mater.,* **259**, 9 (2018).
26. H. He, Y. Yan, J. Huang, J. Lu, *Sep. Purif. Technol.*, **136**, 36 (2014).
27. M. Baysal, K. Bilge, B. Yılmaz, M. Papila, Y. Yürüm, *J. Environ. Chem. Eng.*, **6**, 1702 (2018).
28. S. S. Deshmukh, A. V. Humbe, A. Kumar, R. G. Dorik, K. M. Jadhav, *J. Alloys Compd.,* **704,** 227 (2017).
29. T. S. Tsoncheva, G. S. Issa, A. B. Mileva, R. N. Ivanova, M. D. Dimitrov, I. P. Spassova, D. G. Kovacheva, D. G. Paneva, N. I. Velinov, B. G. Tsyntsarski, N. V. Petrov, *Bulg. Chem. Commun.,* **49**, 167 (2017).
30. T. S. Tsoncheva, I. Genova, I. G. Stoycheva, I. P. Spassova, R. N. Ivanova, B. G. Tsyntsarski, G. S. Issa, D. G. Kovacheva, N. V. Petrov, *J. Porous Mater.,* **22**, 1127 (2015).